Bull Math Biol (2013) 75:1524–1543
DOI 10.1007/s11538-013-9858-x

Society for Mathematical Biology

ORIGINAL ARTICLE

Meniscal Tear Film Fluid Dynamics Near Marx's Line

V.S. Zubkov · C.J.W. Breward · E.A. Gaffney

Received: 8 June 2012 / Accepted: 21 May 2013 / Published online: 3 July 2013

Abstract Extensive studies have explored the dynamics of the ocular surface fluid, though theoretical investigations are typically limited to the use of the lubrication approximation, which is not guaranteed to be uniformly valid a-priori throughout the tear meniscus. However, resolving tear film behaviour within the meniscus and especially its apices is required to characterise the flow dynamics where the tear film is especially thin, and thus most susceptible to evaporatively induced hyperosmolarity and subsequent epithelial damage. Hence, we have explored the accuracy of the standard lubrication approximation for the tear film by explicit comparisons with the 2D Navier–Stokes model, considering both stationary and moving eyelids. Our results demonstrate that the lubrication model is qualitatively accurate except in the vicinity of the eyelids. In particular, and in contrast to lubrication theory, the solution of the full Navier–Stokes equations predict a distinct absence of fluid flow, and thus convective mixing in the region adjacent to the tear film contact line. These observations not only support emergent hypotheses concerning the formation of Marx's line, a region of epithelial cell staining adjacent to the contact line on the eyelid, but also enhance our understanding of the pathophysiological consequences of the flow profile near the tear film contact line.

Keywords Tear film · Marx's line

1 Introduction

The exposed cornea and adjacent conjunctiva of the ocular surface are covered by a protective tear film, which continues beneath the eyelids into the ocular fornices and coats the ocular globe and eyelids, as depicted in Fig. 1. In terms of function, this film

V.S. Zubkov (✉) · C.J.W. Breward · E.A. Gaffney
Mathematical Institute, University of Oxford, Oxford, UK
e-mail: vladimir.s.zubkov@gmail.com

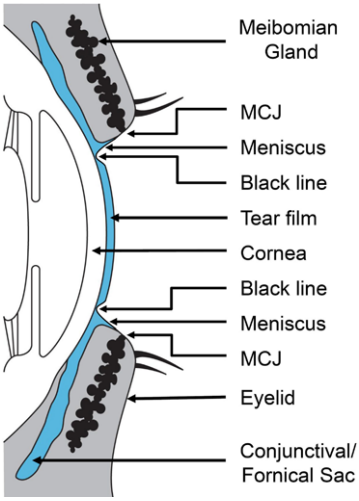

Fig. 1 A schematic of the eye in the sagittal plane, highlighting the tear film, which coats the exposed eyeball and also forms a thin layer in the fornical sac region underneath the eyelids. In addition, at the eyelid margins, a meniscus forms with two apices, one at the *black line* where the meniscus joins the central tear film and the other at mucocutaneous junction (MCJ) in the vicinity of the Meibomian gland ducts. The latter apex forms a contact line, which is pinned due to a change in surface wettability in this region of the eyelid. Note that the depicted meniscus is schematic for clarity rather than to scale. Reproduced, with permission, from Gaffney et al. (2010) (Colour figure online)

inter-alia acts as a protective layer, preventing desiccation of the surface epithelia as well as lubricating eyelid motion during a blink. In terms of structure, the exposed ocular surface fluid is stratified, with an extremely thin lipid layer immediately facing the atmosphere of thickness 100 nm or less (Bron et al. 2004). Beneath this is an aqueous layer, which is derived from the lacrimal glands with a thickness of about 3 μm (King-Smith et al. 2004), overlying a mucus layer and the glycocalyx of the ocular surface epithelium. The tear film also forms a meniscus at the eyelids, wetting up to an apex at the mucocutaneous junction (MCJ) that is observed, via specular microscopy, to demarcate a change in wettability of the underlying substrate, which in turn is attributed to the boundary between wettable conjunctiva and hydrophobic skin (Bron et al. 2011a). The orifices for the Meibomium glands are also found at this juncture and secrete lipids that ultimately form the outermost layer of the tear film. Consequently, a reservoir of lipid persists at the eyelid margins from which lipids emerge to spread across the tear film with each blink (Yokoi et al. 2008).

A second apex of the meniscus forms at its juncture with the tear film and is referred to as the black line. This represents a very thin region of the tear film that arises due to the action of capillary forces, which tend to induce a flow into the meniscus from the central tear film (Sharma et al. 1998), although surface tension gradients and Marangoni forces also appear to be relevant (Aydemir et al. 2011). Hence, the tear film is at its thinnest at these meniscal apices, i.e. at the mucocutaneous junction and also at the black line. Thus, the effects of evaporation might be expected to be most acute in these regions though desiccation may not be relevant except in more extreme cases where tear film break up occurs. Nonetheless, evaporation offers the

prospect for elevated ocular surface damage due to hyperosmolarity, since aqueous losses induce high physiological salt concentrations, which is recognised both as a hallmark of the common affliction, dry eye, and as a causative factor of ocular surface damage (DEWS 2007; Baudouin 2007; Gilbard et al. 1984, 1989; Huang et al. 1989). Consequently, one may initially expect such damage to be most prevalent at the meniscal apices, where the tear film is thinnest.

However, there is no clear indication of ocular surface damage localised in the vicinity of the black line, in distinct contrast to the mucocutaneous junction. Indeed, detailed evidence has been presented to support the *Marx's line hyperosmolarity hypothesis*, i.e. that hyperosmolarity generated near the mucocutaneous junction is responsible for Marx's line, a zone of epithelial permeability and ocular staining in the conjunctival epithelium in the vicinity of the mucocutaneous junction (Bron et al. 2011a). In addition, these concepts suggest numerous potential clinical implications, for instance in the progression of Meibomium gland disorders, which in turn promote dry eye (Bron et al. 2011b), emphasising the importance of refining our understanding the microenvironmental details of fluid flow and solute transport within the tear film meniscus.

For instance, the Marx's line hyperosmolarity hypothesis requires an assumption that the osmolar microenvironments at the two meniscal apices are substantially different given the absence of ocular staining around the black line. Furthermore, the persistence of hyperosmolarity at the mucocutaneous junction requires that osmolar gradients can be supported in this region, and thus are not eliminated by advective mixing or diffusive transport. However, current measurements of tear film osmolarities or flows are not nearly refined enough to test such assumptions, thus motivating theoretical studies of the underlying biophysics, fluid dynamics, and solute transport in the vicinity of the black line and the mucocutaneous junction.

There have been extensive mathematical and computational studies exploring the dynamics of the tear film, as recently reviewed by Braun (2012). In particular, earlier studies have focussed on tear film dynamics during the interblink, treating the tear film as a Newtonian lubrication film in the sagittal cross section and neglecting evaporation (Wong et al. 1996; Sharma et al. 1998; Miller et al. 2002). Despite these limitations, such papers have nonetheless been successful in describing the formation of black lines, with refinements due to Marangoni forces from gradients in polar lipid concentration (as experimentally evidenced in Berger and Corrsin 1974; Owens and Phillips 2001; King-Smith et al. 2008) appearing later (Aydemir et al. 2011) and providing insight concerning the observed upward motion of the surface of the tear film after the eyelid motion has ceased. Extensions have included (i) the consideration of evaporation and van der Waals forces, leading to the prediction of an equilibrium fluid layer that wets the corneal surface (Winter et al. 2010), (ii) the draining of the tear film (including polar lipids) during a blink cycle (Jones et al. 2005, 2006; Aydemir et al. 2011), (iii) more accurate, higher dimensional tear film geometries (Maki et al. 2010a, 2010b), and (iv) the influence of non-polar lipids (Breward et al. 2012). However, this body of work has not focussed on the questions emerging from the detailed consideration of hyper-osmolarity and its impact on the ocular surface.

Focussing on this topic, Gaffney et al. (2010) presented a compartmental model for tear film osmolarity on the timescales appropriate to pathology rather than a single

blink, in which the spatial heterogeneity of ocular surface osmolarity for the interpretation of dry eye diagnostic data. A further study (Zubkov et al. 2012) resolved solute transport throughout the central tear film and black line during a blink cycle, incorporating both the polar lipid and aqueous dynamics and demonstrated that relatively high osmolarities are predicted at the black line, though these can be ameliorated by ocular eye movements such as saccades. Nonetheless, it raises the question of whether the osmolar microenvironment near the mucocutaneous junction is even more adverse compared with the micro-environment near the black lines, as required for Marx's line hyper-osmolarity hypothesis. However, all theoretical studies of the fluid dynamics to date have relied upon the lubrication approximation, but in the context of characterising tear film behaviour near Marx's line and the mucocutaneous junction, this is problematic for several reasons:

- The aspect ratio of the meniscus is in fact of order one and, more importantly, the standard lubrication theory framework of tear film dynamics fails to locally respect the no-slip boundary conditions at the eyelid margin. Thus, to explore the fluid dynamics near the mucocutaneous junction, one has to resolve the flow without resorting to the standard lubrication approximation of tear film dynamics (e.g. Wong et al. 1996; Sharma et al. 1998).
- On meniscal lengthscales during the fast dynamics of a blink or a saccade, the Reynolds number is no longer much smaller than unity, and hence inertia should not be neglected.

Thus, in this paper, we focus on the Navier–Stokes flows associated with meniscal tear film dynamics and how they differ from lubrication flows, especially near the mucocutaneous junctions. In particular, our objective is to explore the flow profiles in the vicinity of the meniscal apices and whether our predictions support, or conflict with, the assumptions underlying the Marx's line hyperosmolar hypothesis. We will also assess the limitations of the lubrication assumption in tear film dynamics.

Thus, in Sect. 2, we formulate the Navier–Stokes and lubrication equations of tear film flow, which are explored and compared in Sect. 3 for the cases of moving and stationary eyelids. We discuss our conclusions in Sect. 4, characterising the limitations of lubrication theory and placing our studies in the context of the Marx's line hyperosmolar hypothesis.

2 Model Formulation

2.1 Model of the Tear Film

Following the standard framework for modelling the ocular tear film (e.g. Sharma et al. 1998; Wong et al. 1996; Aydemir et al. 2011), we suppose that the tear film only has an aqueous component and we neglect evaporation and the curvature of the eyeball. We assume the geometry is given by a sagittal cross section and depicted in Fig. 2. Implicit in this framework is the assumption that the eyelid in sagittal cross section can be represented geometrically as a simple rectangle aligned with the ocular surface as depicted. Hence, detailed anatomical features, such as rounding of the

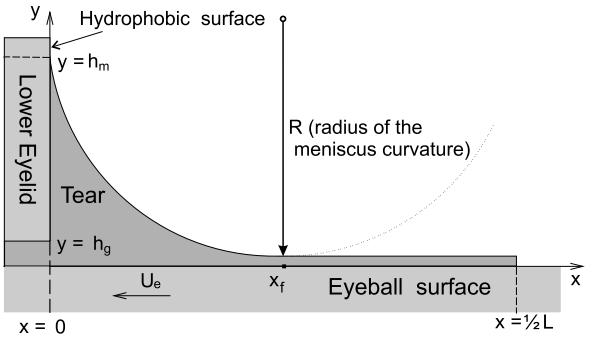

Fig. 2 The figure shows a schematic of the model domain near the lower eyelid

eyelid to form a wiper, with an eyelid margin making an acute angle with the ocular surface (Bron et al. 2011a; Knop et al. 2011), are neglected. Further note that we are considering open eyelids and a domain adjacent to the lower meniscus, based on an assumption that the tear film behaviour near one eyelid does not influence the tear film behaviour near another eyelid. This is an approximation and does not persist through a blink as previously demonstrated (Zubkov et al. 2012); finally, we neglect gravity throughout (which is consistent with a supine posture for example).

In the schematic presented in Fig. 2, the x-axis of the (x, y) coordinate system is aligned with the eyeball surface and the origin is located at the position of the lower eyelid. We also introduce the similarly oriented velocity field of the aqueous component, $\mathbf{u} = (u, v)$ and the tear film thickness h.

We treat the tear fluid as an incompressible Newtonian liquid with constant viscosity and density. Thus, the layer is governed by the Navier–Stokes equations,

$$\begin{aligned} \nabla \cdot \mathbf{u} &= 0, \\ \rho\big[\mathbf{u}_t + (\mathbf{u} \cdot \nabla \mathbf{u})\big] &= -\nabla p + \mu \nabla^2 \mathbf{u}, \end{aligned} \tag{1}$$

where ρ is the density, p is the pressure and μ is the viscosity. Here and below, subscripts t, x, and y are used to denote corresponding partial derivatives. The no-slip condition at the eyeball is

$$u = U_e, \qquad v = 0 \quad \text{at } y = 0, \tag{2}$$

where U_e is the eyeball velocity relative to the eyelid.

Using mass conservation, we write the kinematic condition at the air-tear interface in the form,

$$h_t + \frac{\partial}{\partial x} \int_0^h u \, \mathrm{d}y = 0. \tag{3}$$

The stress balance at the free surface reads

$$\mathbf{n} \cdot (\mathbf{S} \cdot \mathbf{n}) = \gamma \kappa \quad \text{and} \quad \mathbf{t} \cdot (\mathbf{S} \cdot \mathbf{n}) = 0 \quad \text{at } y = h, \tag{4}$$

where γ is the constant surface tension,

$$\kappa = \frac{h_{xx}}{(1 + h_x^2)^{3/2}}, \qquad \mathbf{n} = \frac{(-h_x, 1)}{\sqrt{1 + h_x^2}}, \qquad \mathbf{t} = \frac{(1, h_x)}{\sqrt{1 + h_x^2}}, \tag{5}$$

are respectively the curvature of the free tear surface, the unit normal, and the tangent to the surface, and

$$\mathbf{S} = \begin{bmatrix} -p + 2\mu u_x & \mu(u_y + v_x) \\ \mu(u_y + v_x) & -p + 2\mu v_y \end{bmatrix}, \tag{6}$$

denotes the stress tensor.

The wetting of the eyelid and pinning the contact line under normal circumstances can be observed via specular microscopy, as reported, albeit parenthetically, by Bron et al. (2011a); this structure is attributed to the demarcation between wettable conjuctiva and hydrophobic skin at the mucocutaneous junction. Thus, we assume that the tear film is pinned at this location, and hence we define

$$h(0, t) = h_m, \tag{7}$$

as illustrated in Fig. 2. At the eyelids, we assume that there is no flux along or through the eyelid margins and that liquid is supplied from under the eyelid via a Couette flow,

$$u(x = 0) = \begin{cases} 0, & y \in (h_g, h_m), \\ U_e(1 - \frac{y}{h_g}), & y \in (0, h_g), \end{cases} \tag{8}$$

where h_g is the height of the gap between the ocular surface and the eyelid. In practice, this gap height may vary during eyelid motion, for example as the force exerted by the eyelid muscles varies. However, for simplicity and in the absence of experimental data, we assume that h_g is constant. (The region under the eyelid could be included within the problem domain to describe the tear flow more extensively. However, the Couette flow approximation on matching into the fornical region under the eyelid is a self-consistent and reasonable simplification, based on the assumption that the flow in this region is driven and dominated by the relative motion of the eyelid and eyeball, if any.)

In our simulations, we consider only a small displacement of the eyelid relative to the ocular surface. Thus, we assume that changes in the tear film close to one eyelid do not influence the behaviour of the tear film close to the other one. This movement can arise from a small vertical saccade of a few degrees, which for definiteness we take to be downward. Following Yarbus (1967), we assume that velocity of the eyeball in the reference frame fixed to the *lower* eyelid during a downward vertical saccade is

$$U_e(t) = -U \sin\left(\pi \frac{t - t_{\text{sac}}}{\tau_{\text{sac}}}\right), \quad U = \omega R_{\text{eye}} \text{ for } t_{\text{sac}} \le t \le t_{\text{sac}} + \tau_{\text{sac}}, \tag{9}$$

where ω and R_{eye} are, respectively, the peak angular speed of the eyeball and its radius, with t_{sac} and τ_{sac} denoting the initial time of the saccade and its duration.

At the right boundary, $x = \frac{1}{2}L$, corresponding to half the distance between the open eyelids, we assume that the free surface in this region is in the far field of the meniscus, that is the free surface is flat with a velocity dominantly driven by only the eyeball motion. This is motivated by the fact the lengthscale of the eyelid separation, $L \sim 10^{-2}$m, is much greater than the extent of the motion in the modelled vertical saccade, $\omega R_{\text{eye}} \tau_{\text{sac}}/\pi \sim 6.4 \times 10^{-4}$ m, and also the lengthscales of the meniscus, as

characterised by its radius of curvature and depth $R, h_g \sim 3\text{–}4 \times 10^{-4}$ m. Thus, we have

$$h_x\left(\tfrac{1}{2}L, t\right) = 0 \quad \text{and} \quad u\left(\tfrac{1}{2}L, t\right) = U_e, \quad v\left(\tfrac{1}{2}L, t\right) = 0, \tag{10}$$

which also highlights that we are explicitly modelling only the flow field of the lower meniscus and its matching into the central tear film for a saccade. Further, for the initial free surface shape, we assume that the meniscus curvature, κ, is constant, and given by $1/R$, and that the tear film has a constant thickness l, with these profiles meeting at $x = x_f$.[1] Finally, measuring pressure relative to the atmosphere and taking into account stress balance equations (4), we assume that initial conditions are

$$u = 0, \qquad v = 0, \qquad p = \begin{cases} -\gamma/R, & x \in (0, x_f), \\ 0, & x \in (x_f, \tfrac{1}{2}), \end{cases} \qquad U_e = 0. \tag{11}$$

2.2 Full Non-dimensional Model

Defining $\varepsilon = l/L$ and picking the velocity scale $U = \omega R_{\text{eye}}$, we introduce the following non-dimensional variables:

$$\begin{gathered} x' = \frac{x}{L}, \qquad y' = \frac{y}{\varepsilon L}, \qquad t' = \frac{Ut}{L}, \qquad u' = \frac{u}{U}, \\ v' = \frac{v}{\varepsilon U}, \qquad p' = \frac{\varepsilon^2 L}{\mu U} p, \qquad h' = \frac{h}{\varepsilon L} \end{gathered} \tag{12}$$

and non-dimensional functions and constants

$$h'_m = \frac{h_m}{\varepsilon L}, \qquad h'_g = \frac{h_g}{\varepsilon L}, \qquad U'_e = \frac{U_e}{U}, \qquad R' = \frac{\varepsilon R}{L}, \qquad x'_f = \frac{x_f}{L}. \tag{13}$$

Substituting (12)–(13) into the model (1)–(9), we obtain (primes are omitted)

$$\varepsilon^2 Re\left(\frac{\partial u}{\partial t} + u\frac{\partial u}{\partial x} + v\frac{\partial u}{\partial y}\right) + \frac{\partial p}{\partial x} = \left(\varepsilon^2 \frac{\partial^2 u}{\partial x^2} + \frac{\partial^2 u}{\partial y^2}\right), \tag{14}$$

$$\varepsilon^4 Re\left(\frac{\partial v}{\partial t} + u\frac{\partial v}{\partial x} + v\frac{\partial v}{\partial y}\right) + \frac{\partial p}{\partial y} = \left(\varepsilon^4 \frac{\partial^2 v}{\partial x^2} + \varepsilon^2 \frac{\partial^2 v}{\partial y^2}\right), \tag{15}$$

$$\frac{\partial u}{\partial x} + \frac{\partial v}{\partial y} = 0, \tag{16}$$

while the free surface is given by

$$\frac{\partial h}{\partial t} + \frac{\partial}{\partial x}\int_0^h u \, \mathrm{d}y = 0. \tag{17}$$

The boundary conditions become

$$\begin{cases} C\dfrac{h_{xx}}{(1+\varepsilon^2 h_x^2)^{3/2}} = -p + 2\varepsilon^2 \dfrac{v_y + \varepsilon^2 u_x h_x^2 - h_x(u_y + \varepsilon_x^2 v)}{1 + \varepsilon^2 h_x^2}, \\ 2\varepsilon(v_y - u_x)h_x + \left(u_y + \varepsilon^2 v_x\right)\left(1 - \varepsilon^2 h_x^2\right) = 0, \end{cases} \quad \text{at } y = h, \tag{18}$$

[1] We note at this stage that the value of x_f may be different in the lubrication approximation and the full model.

$$u = U_e, \qquad v = 0 \quad \text{at } y = 0, \tag{19}$$

$$h = h_m \quad \text{at } x = 0, \tag{20}$$

$$u = \begin{cases} 0, & y \in (h_g; h_m), \\ U_e(1 - \frac{y}{h_g}), & y \in (0, h_g), \end{cases} \qquad v = 0 \quad \text{at } x = 0, \tag{21}$$

$$h_x = 0, \qquad u = U_e, \qquad v = 0 \quad \text{at } x = \tfrac{1}{2}, \tag{22}$$

$$U_e(t) = \begin{cases} 0, & t \in (0,\ t_{\text{sac}}), \\ -\sin(\pi \frac{t - t_{\text{sac}}}{\tau_{\text{sac}}}), & t \in (t_{\text{sac}}, t_{\text{sac}} + \tau_{\text{sac}}), \end{cases} \tag{23}$$

and initial conditions

$$\begin{aligned} &u = 0, \qquad v = 0, \qquad p = \begin{cases} -\gamma/R, & x \in (0, x_f), \\ 0, & x \in (x_f, \frac{1}{2}), \end{cases} \\ &h : \begin{cases} \kappa = 1/R, & x \in (0,\ x_f), \\ h = 1, & x \in (x_f, \frac{1}{2}), \end{cases} \quad \text{at } t = 0, \end{aligned} \tag{24}$$

where

$$Re = \frac{\rho U L}{\mu}, \qquad C = \frac{\gamma \varepsilon^3}{\mu U}$$

are the Reynolds number and reduced Capillary number, respectively.

2.3 Lubrication Model

Assuming that ε^2 and $\varepsilon^2 Re$ are small and following the usual routine of lubrication analysis (see the "zero shear stress" model derivation by Jones et al. 2005), the dynamics of the tear film is found to be governed by the following equation:

$$h_t + \left(\frac{1}{3} C h^3 h_{xxx} + U_e h \right)_x = 0, \tag{25}$$

with boundary conditions

$$\begin{aligned} &h(0,t) = h_m, \qquad h_{xxx}(0,t) = -\frac{3U_e}{C h_m^2}\left(1 - \frac{h_g}{2h_m}\right), \\ &h_x\left(\tfrac{1}{2}, t\right) = 0, \qquad h_{xxx}\left(\tfrac{1}{2}, t\right) = 0. \end{aligned} \tag{26}$$

We should note that the lubrication parameter, $\varepsilon = l/L$, is actually understated in the meniscus. Generally speaking, ε is the ratio of the length scale in the y-direction to the length scale in the x-direction. Thus, in the meniscus region, we define $\varepsilon_{\text{meniscus}} = h_m/R$ using the local length scales.[2] As a result, one of the lubrication approximation assumptions, $\varepsilon_{\text{meniscus}} \ll 1$, in fact, is not satisfied—for the normal value of R, $\varepsilon_{\text{meniscus}} \sim O(1)$. However, the lubrication model can work quite well in such circumstances, as seen in Benilov and Zubkov (2008) for $\varepsilon \sim O(1)$.

Now we need to discuss the geometrical difference in the initial conditions for the Navier–Stokes and lubrication models of the problem. In the lubrication case, $\kappa = h_{xx}$ and we thus have

$$h_{xx} = \frac{1}{R}, \tag{27}$$

[2] h_m and R are dimensional in this expression.

in the meniscus coupled with a flat film i.e.

$$h = \begin{cases} \frac{1}{2R}x^2 - \sqrt{\frac{2(h_m-1)}{R}}x + h_m, & x \in (0, x_f), \\ 1, & x \in (x_f, \frac{1}{2}), \end{cases} \quad \text{at } t = 0, \tag{28}$$

where

$$x_f = \sqrt{2(h_m - 1)R}. \tag{29}$$

In the Navier–Stokes model, the curvature condition results in a meniscus free surface which is an arc of a circle and so the initial condition is given by

$$h = \begin{cases} \frac{1}{\varepsilon^2}R + 1 - \frac{1}{\varepsilon^2}\sqrt{R^2 - \varepsilon^2(x - x_f)^2}, & x \in (0, x_f), \\ 1, & x \in (x_f, \frac{1}{2}), \end{cases} \quad \text{at } t = 0, \tag{30}$$

where

$$x_f = \sqrt{2(h_m - 1)R - \varepsilon^2(h_m - 1)^2}. \tag{31}$$

Comparing (29) and (31), we see that x_f is further from the eyelid in the lubrication approximation than in the full model.

Instead of fixing the meniscus radius of curvature, R, in the initial conditions one could instead fix the meniscus volume, V_0, given by

$$\int_0^{x_f} h \, \mathrm{d}x = V_0, \tag{32}$$

where x_f can be easily found. However, we do not consider this case. For the lubrication approximation, the parabolic meniscus leads to a smaller radius of curvature near the black line, $x = x_f$, generating an artefact of enhanced capillary suction into the meniscus relative to the Navier–Stokes model. In turn, this entails the lubrication model then has an unrealistically fast tear film thinning near the black line, leading to an artefact exaggeration of the differences between the two models at the black line. Hence, the meniscus radius of curvature, R, is fixed in the initial conditions.

2.4 Parameter Estimation

The dimensional parameters of the model are presented in Table 1, including a summary of their observation or derivation, together with a list of associated non-dimensional parameters and values in Table 2.

As previously discussed, we assume that the liquid flow from under the eyelid moving relative to the eyeball is described by Couette flow, as detailed in (8). However, the height of the gap between the eyeball and the eyelid, h_g, is not known. We therefore use an a posteriori reference value of $h_g = 6 \times 10^{-6}$ m. A gap of this height produces an aqueous flux from under the eyelids that matches the average rate of deposition for the central tear film given its reported depth of 3 microns (King-Smith et al. 2004).

Taking into account the dependence between the eyelid angular velocity relative to the eyeball, ω, and the saccade duration, τ_{sac}, we use the following dimensional

Table 1 Reference dimensional parameter estimates

Parameter	Value	Notes and citations
Scale for non-dimensionalising the tear film depth, l	3×10^{-6} m	Observation of central tear film depth, King-Smith et al. (2004)
The eyelids separation, L	10^{-2} m	Observation
Angular velocity peak during the saccade, ω	$\frac{4}{3}\pi$ rad/s	Observation, Harwood et al. (1999)
Radius of the eyeball, R_{eye}	0.012 m	Observation
Saccade maximum velocity, U	5.03×10^{-2} m/s	$U = \omega R_{\text{eye}}$
Radius of the meniscus curvature, R	3.65×10^{-4} m	Observation, Yokoi et al. (1999)
Viscosity, μ	1.3×10^{-3} Pa s	See Tiffany et al. (1989)
Gap between ocular surface and eyelids, h_g	6×10^{-6} m	Derived by considering the flux required to lay down a film of depth l in the upblink
Meniscus depth, h_m	2.7×10^{-4} m	Derived. See Johnson and Murphy (2005) and Gaffney et al. (2010)
Surface tension, γ_0	4.5×10^{-2} N/m	See Tiffany et al. (1989)
Density, ρ	1×10^{3} kg/m^3	Density of water
Initial time of a saccade, t_{sac}	2 s	Mid-stage of the interblink
Duration of the saccade, τ_{sac}	0.04 s	See text. Harwood et al. (1999)
End time of the interblink, t_{ib}	5 s	See Tsubota et al. (1996)

Table 2 Reference non-dimensional parameters

Parameter	Value	Interpretation in non-dimensional models
C	1.86×10^{-8}	Inverse capillary number
Re	386.7	Reynolds number
ε	3×10^{-4}	Lubrication parameter
R	1.095×10^{-5}	Radius of the meniscus curvature
h_m	90	Depth of the meniscus
t_{sac}	10.05	Initiation time for the saccade
h_g	2	Gap between the ocular surface and the eyelid
τ_{sac}	0.201	Saccade duration
t_{ib}	25.13	Time of the end of the interblink

values for the peak angular speed of the eyeball during the saccade and the duration of a saccade (Harwood et al. 1999):

$$\omega = \frac{4}{3}\pi \text{ rad/s}, \qquad \tau_{\text{sac}} = 0.04 \text{ s}.$$

2.5 Numerical Methods

In the next section, the Navier–Stokes and lubrication models of tear film flow are compared for the cases of moving and stationary eyelids. In order to obtain the dy-

namics of the tear film, the non-dimensionalised models were solved numerically. The lubrication model equations were integrated using the finite-element-based PDE module of the COMSOL Multiphysics 3.5a, while the Navier–Stokes equations required use of using the Moving Mesh (ALE) and Incompressible Navier–Stokes modules. Steady state solutions of the Navier–Stokes model were obtained as the large time steady state emerging from the time dependent problem, with the initial conditions described in Sect. 2.2. In all cases, it was verified that the solutions were unaffected to within suitable tolerances once the mesh size and time step were sufficiently decreased.

3 Comparison of the Navier–Stokes and the Lubrication Models

3.1 Static Eyelids

First, we consider the evolution of the tear film during the interblink when the eye is open and the position of the eyeball relative to the eyelids is fixed, i.e. $U_e = 0$. Solving the problem numerically for the normal parameters of the tear film, we obtained solutions for the both models. Figure 3(left) shows the tear film profiles for the lubrication model and Navier–Stokes model at the end of interblink, $t_{\text{ib}} = 25.13$ (5 s). The profiles are almost identical, but the minimum for the lubrication model is shifted further from the eyelid. Figure 3(right) shows the thinnest value of the tear film as a function of time during the interblink for the two models, and shows good agreement as expected, given the choice of initial conditions.

Figure 4 demonstrates the convergence of the lubrication model's prediction for the black line thickness and location to that of the Navier–Stokes model as the parameter, $\xi = 1/\varepsilon_{\text{meniscus}}$, or the tear meniscus volume, V_0, increase, which is equivalent to $\varepsilon_{\text{meniscus}} \to 0$. In particular, we present the following measures for the relative

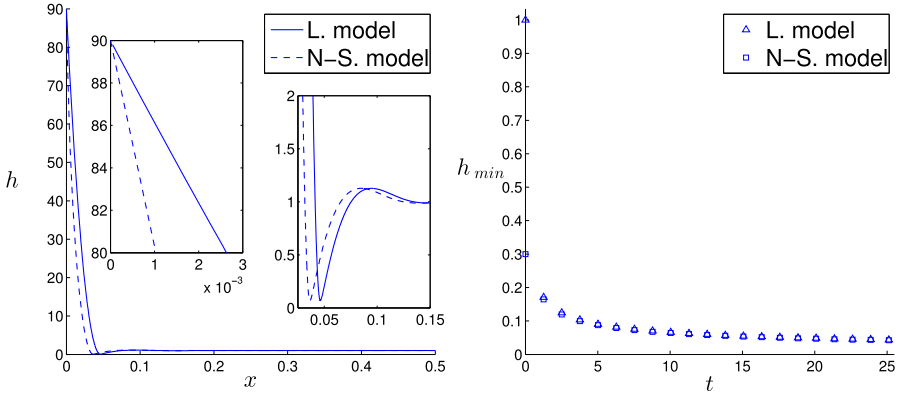

Fig. 3 (*left*) Tear film thickness profile for the Navier–Stokes and lubrication models at the end of interblink, $t_{\text{ib}} = 25.13$ (5 s); (*right*) The minimum value of the tear film thickness as a function of time for the Navier–Stokes and lubrication models

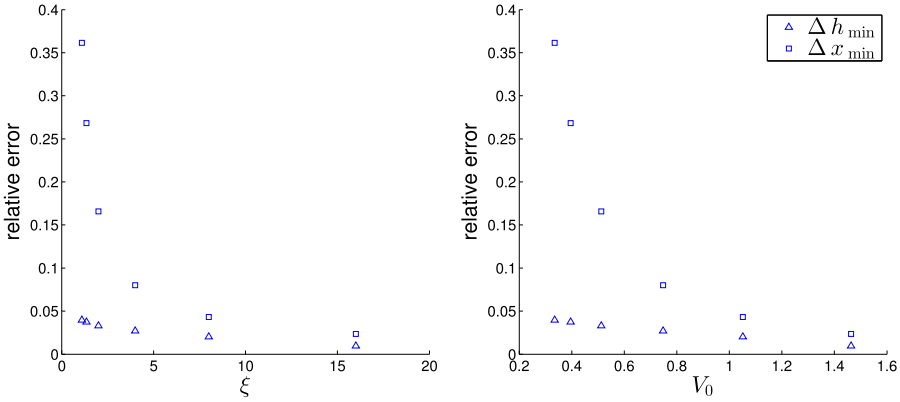

Fig. 4 The figure shows relative deviation $\Delta x_{\min}$ and $\Delta h_{\min}$ of the lubrication approximation from the Navier–Stokes model, as defined by Eqs. (33), for various values of ξ and V_0 given static eyelids. $\Delta h_{\min}$ represents the relative deviation of the minimum tear film thickness for the lubrication model and $\Delta x_{\min}$ represents the relative deviation of the corresponding x-coordinate of the minimum point

deviation for the lubrication approximation predictions for black line location and thickness compared to the Navier–Stokes predictions:

$$\Delta x_{\min} = \frac{x_{1\,\min}}{x_{2\,\min}} - 1, \qquad \Delta h_{\min} = \frac{h_{1\,\min}}{h_{2\,\min}} - 1, \tag{33}$$

with

$$h_{i\,\min}(x_{i\,\min}) = \min_{x\in[0,1]} h, \quad i = 1, 2 \text{ at } t = 25.13 \text{ (5 s)}, \tag{34}$$

where $i = 1$ corresponds to the lubrication model and $i = 2$ corresponds to the Navier–Stokes model. Thus, $\Delta h_{\min}$ represents the relative deviation of the minimum tear film thickness for the lubrication model and $\Delta x_{\min}$ represents the relative deviation of the corresponding location of the minimum point across the ocular surface. The deviations for the normal parameters of the tear film correspond to $\xi = 1.352$ in Fig. 4.

One can see that the lubrication model describes the evolution of the tear film free surface quantitatively well in the local region of "black line." However, from a global perspective, we have that lubrication theory predicts a wider meniscus, due to the different profiles, parabolic versus circular, arising in the two models, as previously discussed in the consideration of the initial conditions. We do not present details of the tear behaviour in the meniscus close to the eyelid since there is no noticeable difference between the models for the eyeball fixed relative to the eyelids. Thus, the lubrication model can quantitatively describe the local behaviour of the black line within the interblink and the model converges to the Navier–Stokes model as the meniscus volume increases. We proceed to consider the extended tear film domain in detail during the relative motions of the eyelid and ocular globe, as occurs during blinks and saccadic motions.

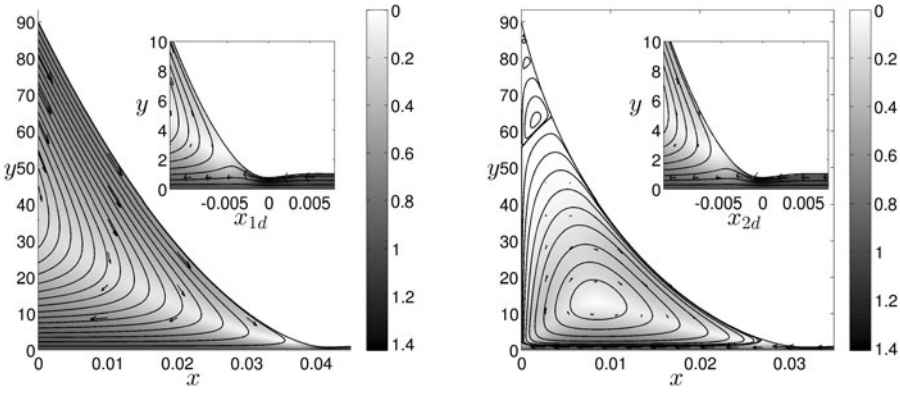

Fig. 5 The absolute speed of the steady state tear flow in the region of the lower meniscus for the lubrication (*left*) and Navier–Stokes (*right*) models when the eyeball surface moves downward with a constant velocity (35). The *black curves* correspond to stream lines and the arrows show directions of the flow with the shifted coordinates x_{1d} and x_{2d} defined in Eq. (36)

3.2 Relative Eyelid Motion

Now, we model the tear film in the case when eyeball moves relative to the eyelid. We consider two cases. In the first one, the velocity of the eyelid is constant so that the velocity profile reaches its steady state profile; while unrealistic, this nonetheless reveals the nature of the mixing processes in the tear meniscus. In the second case, the velocity of the eyeball is an empirically motivated function of time, as defined in Eq. (23).

3.2.1 Tear Film Behaviour for the Eyeball Moving with a Constant Velocity

First, we considered the model when the eyeball surface moves downward with a constant velocity,

$$U_e = -1. \tag{35}$$

Solving the full Navier–Stokes model (14)–(22), (24), (30), (31) and lubrication equations (25), (26), (28), (29) numerically, we obtained steady states profiles. Figure 5 shows the absolute value of the tear velocity in the region of the lower meniscus for the lubrication model (left) and Navier–Stokes model (right). The black curves show the stream lines and the arrows show direction of the flow.

The subplots in Fig. 5 show the flow in the region of the black lines with shifted x-coordinate,

$$x_{id} = x - x_{i\,\min}, \quad i = 1, 2, \tag{36}$$

where $x_{i\,\min}$ is defined in (34), so that the black lines are in both subplots are located at $x_{id} = 0$. Comparing results near the new origins, we see that they are identical at visible resolution. However, the two models predict significantly different free surface profiles and flows in the meniscus. In the lubrication model, the flow is not zero at the lower eyelid and the absolute value of the tear velocity is relatively large in the

whole meniscus. In contrast, for the Navier–Stokes model, we see a much steeper free surface profile near the mucocutaneous junction and in particular, multiple vortices and much smaller velocities throughout most of the meniscus with the absolute value of the tear velocity tending to zero at the upper corner. The infinite series of vortices in the Navier stokes solution have been previously described analytically by Moffatt (1963) for a flow in the corner of two straight boundaries and the third opposite moving boundary and separate the fluid in the mucocutaneous junction region from the bulk meniscus. It is not surprising that the predicted behaviour in this region is different for the two models, since we are unable to apply the no-slip boundary condition (21) in the lubrication model. We expect that the lubrication flow is an 'outer solution' and it is clearly valid near the black line. However, when details such as the meniscus shape or flow profile are required it is clear that this outer solution is not valid for the majority of the meniscus and hence lubrication theory significantly misrepresents the shape, volume, fluid flow, and thus advective mixing associated with the meniscus.

3.2.2 Tear Film Behaviour in a Vertical Saccade

Now, we look at the case when the eyeball moves downward in a vertical saccade with velocity defined by (23) following a two second period of interblink with the eyeball fixed. The full Navier–Stokes model (14)–(24), (30), (31) and lubrication equations (25), (26), (28)–(29) were solved numerically. Figure 6 shows absolute value of the tear velocity in the region of the meniscus for the two models. The results correspond to (a) the beginning of the saccade, $t = 10.08$ (2.005 s); (b) the middle of the saccade, $t = 10.15$ (2.02 s), when the eyeball velocity is maximum and (c) the ending of the saccade, $t = 10.23$ (2.035 s).

Figure 7 shows the tear film profiles for the two models and thinning of the tear film at the black line with time. Similarly to Fig. 4, Fig. 8 confirms convergence of the lubrication model's prediction for the height and location of the black line to the Navier–Stokes model as the tear volume increases.

Figures 6 and 7 demonstrate that the two models predict similar behaviour in the vicinity of black line with the overestimate for the position of black line in the lubrication approximation. In particular, the insets of Fig. 6 demonstrates that the lubrication approximation captures the local dynamics near the black line.

However, as described for the constant eyeball velocity case, the tear flows and the predicted shapes of the free surface are different in the meniscus. Firstly, the meniscus volume is less for the Navier–Stokes predictions and, in particular, the free surface profile is much steeper in the vicinity of the mucocutaneous junction, especially on noting the different horizontal lengthscales on the axes in Fig. 6. Further, all of the smaller Moffatt vortices have been suppressed by a small movement of the meniscus free surface due to the saccade. Looking at the streamlines of the flow calculated using the Navier–Stokes model, we see that at the beginning of the saccade the free surface of the meniscus upper part moves up (Fig. 6, a), whereas at the end of the saccade it moves down (Fig. 6, c). While we no longer observe the multiple vortices in the Navier–Stokes predictions, we see that streamlines do not connect the region of the mucocutaneous junction to the bulk meniscus. In addition, the absolute velocity

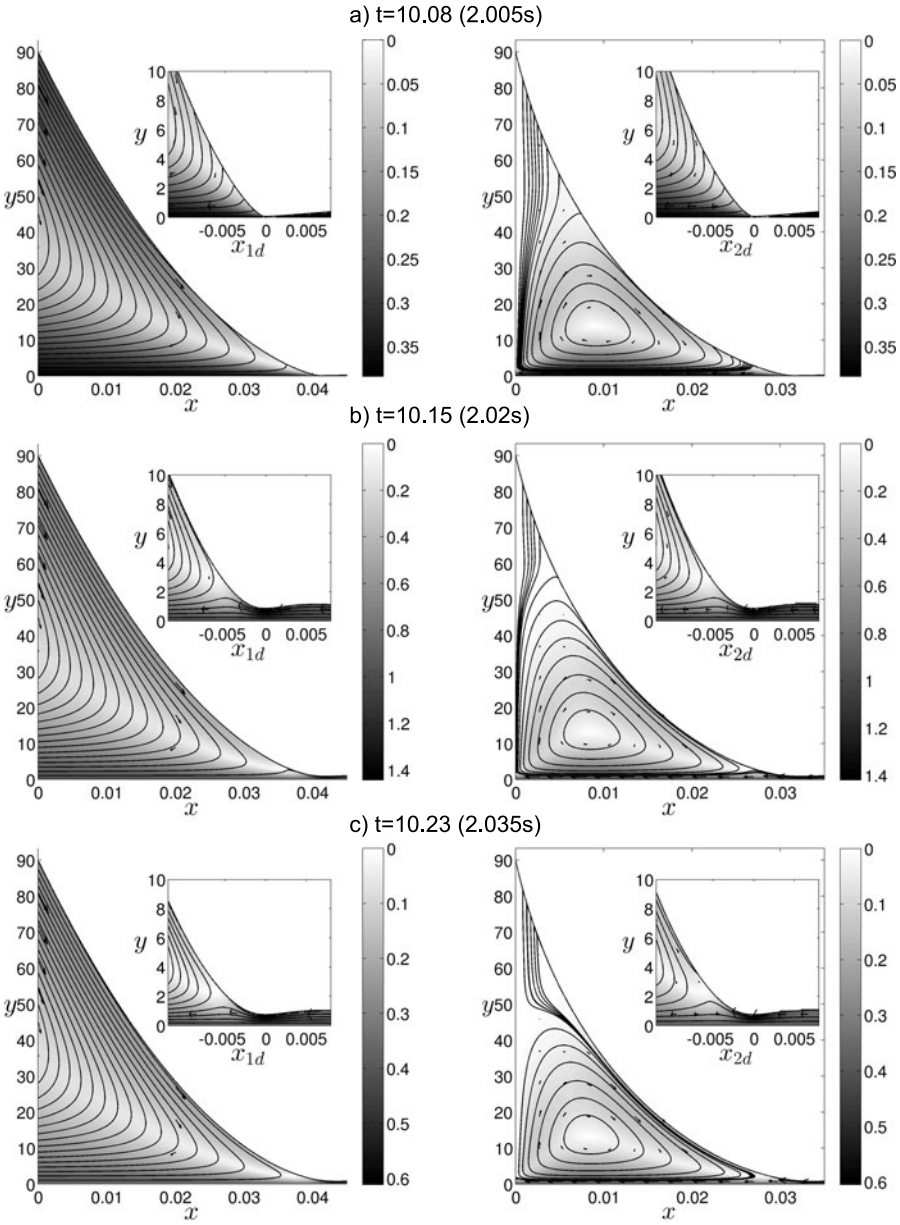

Fig. 6 The absolute speed of the tear flow in the region of the lower meniscus for the lubrication (*left*) and Navier–Stokes (*right*) models when the eyeball moves downward in the vertical saccade (23) after 2 seconds of interblink. The duration of the saccade is 0.04 seconds. The results correspond to (**a**) the beginning of the saccade, $t = 10.08$ (2.005 s); (**b**) the middle of the saccade, $t = 10.15$ (2.02 s), when the eyeball velocity is maximum and (**c**) the ending of the saccade, $t = 10.23$ (2.035 s). The *black curves* correspond to stream *lines* and the *arrows* show directions of the flow with the shifted coordinates x_{1d} and x_{2d} defined in Eq. (36)

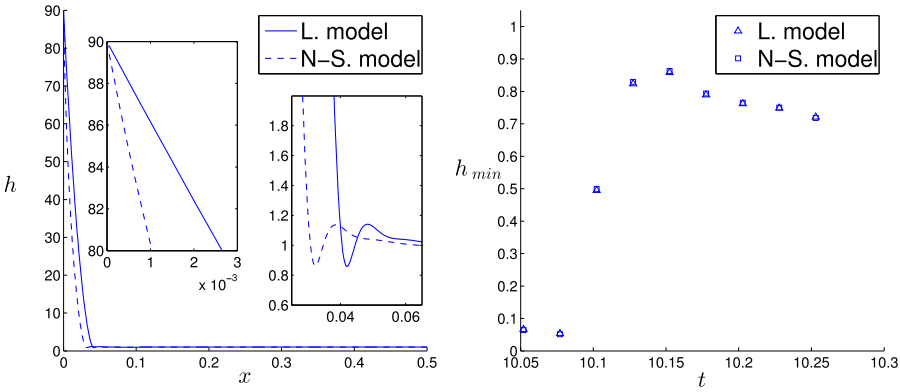

Fig. 7 (*left*) Tear film thickness profile for the Navier–Stokes and lubrication models in the middle of the saccade, $t = 10.15$ (2.02 s); (*right*) Tear film minimum thickness at the lower lid margin as a function of time for the Navier–Stokes and lubrication models

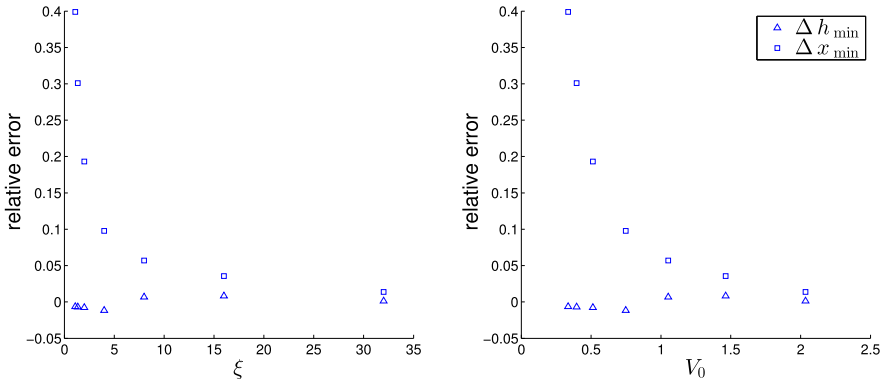

Fig. 8 The figure shows relative deviation $\Delta x_{\min}$ and $\Delta h_{\min}$ of the lubrication approximation from the Navier–Stokes model, as defined in Eq. (33), for various values of ξ and V_0 given an eyeball motion corresponding to a downward vertical saccade, as defined by Eq. (23). The results represent the middle of the saccade, $t = 10.15$ (2.02 s), when the eyeball velocity is maximum. Note that $\Delta h_{\min}$ represents the relative deviation of the minimum tear film thickness for the lubrication model and $\Delta x_{\min}$ represents the relative deviation of the corresponding x-coordinate of the tear film minimum

value of the tear flow drops by a factor of $O(10^3)$ on moving from the main vortex of the meniscus to the mucocutaneous junction giving extremely small dimensional velocity scales in this region, of about $10^{-3}U \sim 5 \times 10^{-5}$ m/s.

In our simulations, we decreased the gap between the eyeball and the eyelid, h_g, to zero, and as a result the meniscus volume increased. This is because we closed the gap for outflow from the meniscus and kept the inflow coming with the tear film at the eyeball surface during the saccades. As a result, we observed a small increase in the meniscus thickness. However, this increase has not changed the picture of the flow or free surface profile meaningfully, and thus does not impinge on our conclusions.

4 Discussion and Conclusions

In this paper, we considered the dynamics of a tear film during (i) an interblink when the eyelids are open and fixed relative to the eyeball, (ii) a constant velocity between the ocular surface and the eyelid and (iii) a small relative eyeball motion as in the case of a vertical saccade. We compared the results of the numerical simulations for the 2D Navier–Stokes and standard lubrication models of the tear film, where lengthscales perpendicular to the ocular surface are much smaller than those along the ocular surface. However, for simplicity, we only consider the half of the domain that includes the tear film near the lower eyelid.

Our results demonstrate that the lubrication model accurately captures the local behaviour near the black line, though it overestimates the position of the black line, predicting it to be further from the eyelid. For the normal tear parameters and both the static and saccadic cases, the difference in the tear film thickness is small, 4 % or less, while the black line location is predicted to within 30 %, and our simulations confirm these deviations tend toward zero as the tear volume is increased. As such, lubrication theory is acting as an accurate outer solution for the fluid dynamical behaviour in the meniscus and this is a common feature of both the static and saccadic studies. Thus, if the focus is to resolve black line dynamics or central tear film dynamics not only is lubrication theory appropriate it is, by Occam's razor, highly preferable.

However, away from the black line region within the meniscus, the Navier–Stokes and lubrication theories yield significantly different results in both the static and saccadic cases. Firstly, the meniscus profile is predicted to be very different, as one might anticipate in that a static meniscus is parabolic according to lubrication theory but circular according to the Navier–Stokes equations. Nonetheless, this has important implications for tear film modelling. Firstly, for the accurate prediction of capillary forces in the meniscus, lubrication theory overestimates meniscal volumes. However, this means the influence of evaporation is likely to be underestimated since the surface area to volume ratio is distorted and thus lubrication theory models may systematically underestimate meniscal osmolarities in solute balance models. Secondly, near the mucocutaneous junction, such discrepancies appear to be even more extreme for both the static and dynamic meniscus. In particular, the Navier–Stokes equations predict a much steeper ascent of the free surface into the mucocutaneous junction, leading to a much thinner film in this region. In turn, the associated unfavourable surface area to volume ratio in this region will exacerbate the effects of evaporation and such influences are hypothesised to be important in the formation of Marx's line (Bron et al. 2011a).

Such discrepancies, in isolation, are possibly be remedied by modifying the lubrication approximation to include the full curvature of the free tear surface (Wilson 1982), resulting in models which have a similar structure to the lubrication theory model. However, the discrepancies with the lubrication approximation are more extensive than simply the profile of the free surface and it does not provide an accurate description of the fluid dynamics within the interior of the tear meniscus in the saccadic case. The Navier–Stokes equations clearly predict a vortex leading to extensive mixing within the bulk of the meniscus, with negligible fluid flow and advective mixing near the mucocutaneous junction, in distinct contrast to the lubrication theory

predictions. In particular, the extreme drop in velocity, by a factor of 10^3 to a scale of 5×10^{-5} m/s, on approaching the mucocutaneous junction within the Navier–Stokes prediction has no analogue within the lubrication theory model. Thus lubrication theory does not suggest any absence of advective transport in the vicinity of the mucocutaneous junction. In contrast for the Navier–Stokes simulation with the timescale of a saccade, about 0.04 s, the lengthscale of advective transport in the vicinity of the mucocutaneous junction is about 2 microns, and thus appears to be essentially absent even on cellular scales.

This supports the idea that there is severely restricted advective solute transport between the bulk meniscus and the region of the mucocutaneous junction in distinct contrast to the black line, where flow is continually refreshed from the relatively thick central corneal tear film. Hence, advective transport continually dilutes the fluid in the vicinity of the black line, in contrast to the mucocutaneous junction, emphasising the osmolar microenvironments of the meniscal apices are different. This, together with the restricted advective transport in the vicinity of the mucocutaneous junction, is required for the validity of the Marx's line hyperosmolar hypothesis but only emerges on the consideration of the Navier–Stokes equations.

We cannot comment on further requirements of Marx's line hyperosmolar hypothesis, such as the influence of diffusive transport and evaporation within the current study. Thus, a clear extension is the inclusion of evaporation and lipid dynamics together with solute transport to further investigate the Marx's line hyperosmolar hypothesis. For example, errors in the lubrication approximation for flows in the vicinity of the mucocutaneous junction may additionally influence lipid redistribution and thus evaporation in this region. Such considerations, together with the observations we have presented, emphasise that future studies of osmolarity in the vicinity of the mucocutaneous junction to assess the Marx's line hyperosmolar hypothesis and its associated clinical implications (Bron et al. 2011a, 2011b) cannot rely upon the standard modelling framework of tear film lubrication theory presented thus far in the literature. Nonetheless, this does not detract from the usefulness of lubrication theory for studies where the focus does not require resolving the detailed flow near the eyelid margins or the precise meniscus shape.

Acknowledgements This paper is based on work supported by Award No. KUK-C1-013-04 made by King Abdullah University of Science and Technology (KAUST). We are grateful to Professor Richard Braun, Professor Anthony Bron, Professor Colin Please, and Dr. John Tiffany for insightful discussions.

References

Aydemir, E., Breward, C. J. W., & Witelski, T. P. (2011). The effect of polar lipids on tear film dynamics. *Bull Math Bio*, *73*(6), 1171–1201.

Baudouin, C. (2007). The vicious circle in dry eye syndrome: a mechanistic approach. *J. Fr. Ophthalmol.*, *30*, 239–246.

Benilov, E., & Zubkov, V. (2008). On the drag-out problem in liquid film theory. *J. Fluid Mech.*, *617*, 283–299.

Berger, R. E., & Corrsin, S. (1974). A surface tension gradient mechanism for driving the pre-corneal tear film after a blink. *J. Biomech.*, *7*, 225–238.

Braun, R. J. (2012). Dynamics of the tear film. *Annu. Rev. Fluid Mech.*, *44*, 267–297.

Breward, C. J. W., Bruna, M., Gaffney, E. A., & Zubkov, V. S. (2012, in preparation). The influence of nonpolar lipids on tear film dynamics.

Bron, A., Tiffany, J., Gouveia, S., Yokoi, N., & Voon, L. (2004). Functional aspects of the tear film lipid layer. *Exp. Eye Res.*, *78*, 347–360.

Bron, A. J., Yokoi, N., Gaffney, E. A., & Tiffany, J. M. (2011a). A solute gradient in the tear meniscus I. An hypothesis to explain Marx's line. *Ocul. Surf.*, *7*, 92–97.

Bron, A. J., Yokoi, N., Gaffney, E. A., & Tiffany, J. M. (2011b). A solute gradient in the tear meniscus II. Implications for lid margin disease, including Meibomian gland dysfunction. *Ocul. Surf.*, *9*, 70–91.

DEWS (2007). The epidemiology of dry eye disease: report of the epidemiology subcommittee of the international dry eye workshop. *Ocul. Surf.*, *5*, 93–107.

Gaffney, E. A., Tiffany, J. M., Yokoi, N., & Bron, A. J. (2010). A mass and solute balance model for tear volume and osmolarity in the normal and the dry eye. *Prog. Retin. Eye Res.*, *29*, 59–78.

Gilbard, J. P., Carter, J. B., Sang, D. N., Refojo, M. F., Hanninen, L. A., & Kenyon, K. R. (1984). Morphologic effect of hyperosmolarity on rabbit corneal epithelium. *Ophthalmology*, *91*, 1205–1212.

Gilbard, J. P., Rossi, S. R., & Heyda, K. G. (1989). Tear film and ocular surface changes after closure of the meibomian gland orifices in the rabbit. *Ophthalmology*, *96*, 1180–1186.

Harwood, M. R., Mezey, L. E., & Harris, C. M. (1999). The spectral main sequence of human saccades. *J. Neurosci.*, *19*, 9098–9106.

Huang, A. J. W., Belldegrun, R., Hanninen, L., Kenyon, K. R., Tseng, S. C. G., & Refojo, M. F. (1989). Effect of hypertonic solutions on conjunctival epithelium and mucin like glycoprotein discharge. *Cornea*, *8*, 15–20.

Johnson, M. E., & Murphy, P. J. (2005). The agreement and repeatability of tear meniscus height measurement methods. *Optom. Vis. Sci.*, *82*, 1030–1037.

Jones, M. B., Please, C. P., McElwain, D. L. S., Fulford, G. R., & Robert, A. P. (2005). Dynamics of tear film deposition and draining. *Math. Med. Biol.*, *22*, 265–288.

Jones, M. B., Please, C. P., McElwain, D. L. S., Fulford, G. R., & Robert, A. P. (2006). The effect of the lipid layer on tear film behaviour. *Bull. Math. Biol.*, *86*, 1355–1381.

King-Smith, P. E., Fink, B. A., Hill, R. M., Koelling, K. W., & Tiffany, J. M. (2004). The thickness of the tear film. *Curr. Eye Res.*, *29*, 357–368.

King-Smith, P. E., Nichols, J. J., Nichols, K. K., Fink, B. A., & Braun, R. J. (2008). Contributions of evaporation and other mechanisms to tear film thinning and break-up. *Optom. Vis. Sci.*, *85*, 623–630.

Knop, E., Knop, N., Zhivov, A., Kraak, R., Korb, D., Blackie, C., Greiner, J., & Guthoff, R. (2011). The lid wiper and muco-cutaneous junction anatomy of the human eyelid margins: an in vivo confocal and histological study. *J. Anat.*, *218*, 449–461.

Maki, K. L., Braun, R. J., Henshaw, W. D., & King-Smith, P. E. (2010a). Tear film dynamics on an eye-shaped domain i: pressure boundary conditions. *Math. Med. Biol.*, *27*, 227–254.

Maki, K. L., Braun, R. J., Henshaw, W. D., & King-Smith, P. E. (2010b). Tear film dynamics on an eye-shaped domain part 2. flux boundary conditions. *J. Fluid Mech.*, *647*, 361–390.

Miller, K. L., Polse, K. A., & Radke, C. J. (2002). Black-line formation and the "perched" human tear film. *Curr. Eye Res.*, *25*, 155–162.

Moffatt, H. K. (1963). Viscous and resistive eddies near a sharp corner. *J. Fluid Mech.*, *18*(1), 1–18.

Owens, H., & Phillips, J. R. (2001). Spreading of the tears after a blink - velocity and stabilization time in healthy eyes. *Cornea*, *20*(5), 484–487.

Sharma, A., Tiwari, S., Khanna, R., & Tiffany, J. M. (1998). Hydrodynamics of meniscus induced thinning of the tear fluid. In D. Sullivan, D. Dartt, & M. Meneray (Eds.), *Lacrimal gland, tear film, and dry eye syndromes* (p. 2). New York: Plenum.

Tiffany, J. M., Winter, N., & Bliss, G. (1989). Tear film stability and tear surface tension. *Curr. Eye Res.*, *8*, 507–515.

Tsubota, K., Hata, S., Okusawa, Y., Egami, F., Ohtsuk, T., & Nakamori, K. (1996). Quantitative videographic analysis of blinking in normal subjects and patients with dry eye. *Arch. Ophthalmol.*, *114*, 715–720.

Wilson, S. D. R. (1982). The drag-out problem in film coating theory. *J. Eng. Math.*, *16*, 209–221.

Winter, K. N., Anderson, D. M., & Braun, R. J. (2010). A model for wetting and evaporation of a post-blink precorneal tear film. *Math. Med. Biol.*, *27*, 211–225.

Wong, H., Fatt, I., & Radke, C. J. (1996). Deposition and thinning of the human tear film. *J. Colloid Interface Sci.*, *184*, 44–51.

Yarbus, A. L. (1967). *Eye movements and vision*. New York: Plenum.

Yokoi, N., Bron, A. J., Tiffany, J. M., Brown, N., Hsuan, J., & Fowler, C. (1999). Reflective meniscometry: A. non-invasive method to measure tear meniscus curvature. *Br. J. Ophthalmol.*, *83*, 92–97.

Yokoi, N., Yameda, H., Mizukusa, Y., Bron, A. J., Tiffany, J. M., Kato, T., & Kinoshita, S. (2008). Rheology of tear film lipid layer spread in normal and aqueous tear-deficient dry eyes. *Investig. Ophthalmol. Vis. Sci.*, *49*, 5319–5324.

Zubkov, V. S., Breward, C. J. W., & Gaffney, E. A. (2012). Coupling fluid and solute dynamics within the ocular surface tear film: a modelling study of black line osmolarity. *Bull. Math. Biol. 74*(9), 2062–2093. doi:10.1007/s11538-012-9746-9.